Printed Periodic Structures in Support to 5G Network Antennas

Printed Periodic Structures in Support to 5G Network Antennas

Aldo De Sabata[1][0000−0002−1821−4977], Ladislau Matekovits[1,2,3#][0000−0003−0946−9561], and Andrei Silaghi[1][0000−0002−8699−1575]

[1] Faculty of Electronics and Telecommunications, Politehnica University Timisoara, 300223 Timisoara, Romania
[2] Department of Electronics and Telecommunications, Politecnico di Torino, 10129 Torino, Italy
[3] Istituto di Elettronica e di Ingegneria dell'Informazione e delle Telecomunicazioni, National Research Council, 10129 Turin, Italy
aldo.de-sabata@upt.ro[+], ladislau.matekovits@polito.it[#], andrei.silaghi@upt.ro[*]

Abstract. Periodic patterns printed on PCBs offer support for enhancement of 5G antennas performance in diversity, isolation, beam-forming and user tracking. Bulky wave processing devices such as dielectric lenses and reflectors can be replaced with such thin and cost-effective structures. These opportunities are addressed in the present chapter in connection to high impedance surfaces, frequency selective surfaces and metasurfaces. The operating principles of these 2D periodic structures are outlined and relevant applications are presented. Since radiating structures must comply with regulations concerning EM interference and human exposure levels, a paragraph is dedicated to a review of the work done to assess and solve these issues.

Keywords: Periodic Structure · Frequency Selective Surface · Metasurface · EM Interference.

1 Introduction

Modern wireless communication systems are facing ever increasing demands for large data volumes, higher data rates (multi Gbps) and throughput, wide spectrum, user's mobility, increased communication reliability, lower latency, and requirements for data convergence. A new generation of mobile communications occurred every ten years in the recent history. In the 5G system, a large variety of services will be provided to a great number of both mobile human and machine-type users [1].

Two frequency bands have been considered of interest for future 5G deployment: the sub-6 GHz range and the mm-wave range, above 24 GHz. The sub-6 GHz range might be subject to interference caused by high-density small-sized cells, and interference with other radio services, such as satellite communications [1]. In the case of mm-wave frequency range, (non) line-of-sight propagation from

the base stations to users is hindered by high attenuation in heavy rain conditions and by attenuation, reflections and fading introduced by urban obstacles such as buildings, walls, vegetation etc [2]. The feasibility of 5G communications at 28 and 38 GHz has been confirmed by measurements in densely populated urban areas and in various weather conditions [3].

In the future 5G paradigm, the antenna end at the base stations will play a key role in providing high quality links, spectrum efficiency, high gain, interference mitigation, directional and adaptive beamforming, and user tracking [3]. Spatial processing such as multiple-input-multiple-output (MIMO) technology, polarization conversion and spatial modulation will enhance the radio frequency (RF) connecting capabilities.

Planar periodic structures implemented on printed circuit boards (PCBs) have been combined with low-profile antennas to achieve highly efficient, directive, and versatile radiating structures. Bulky dielectric lenses and reflectors have been replaced with lower profile transmitarrays and reflectarrays respectively, realized as arrays of elementary scatterers such as dipoles, loops and patches on PCBs, whose re-radiation of the incident wave realizes directionality, focusing or beam-shaping and side-lobe control [4]. Inclusion of active elements allows for beam control in space and time in view of user tracking, replacing the technologically complex electronic control in phased antenna arrays.

However, periodic patterns impressed on PCBs found applications not only as constituents of radiating structures, but also as elements that support the spatial distribution of waves as required by certain applications. For example, in the 5G context, to mitigate interference in the sub-6 GHz band, periodic structures can be developed to confine signals within certain rooms or areas surrounded by walls through selective reflection, while filtering signals coming from the exterior in nearby frequency bands and leaving unaltered signals form other useful frequency bands such as Global System for Mobile Communications (GSM) or Long Term Evolution (LTE) [2]

Besides solving interference issues, these solutions may contribute to increase the degree of confidentiality in confined spaces. Planar periodic patterns set as wallpapers, selective blinds, or incorporated into windows may be deployed for the purpose of mutually insulating access points operating in proximity. Spatial coverage enhancement of base stations inside and outside buildings may be achieved by a smart deployment of planar or conformal, passive or active periodic structures, able to diffusely reflect or transmit incoming waves from the base station antenna in the mm-wave range. FSSs can be also deployed at street intersections to increase non-line-of-sight (NLOS) coverage in urban corridors for mm-wave 5G vehicular communications [2].

The rest of this chapter deals with three engineering solutions pertinent to this topic: high impedance surfaces (HISs), frequency selective surfaces (FSS) and metasurfaces (MS). Moreover, at the end of the chapter some features related to the use of such configurations for electromagnetic (EM) compatibility (EMC)-related issues are discussed. General aspects concerning the impact of EMC requirements on 5G radiating structures are also tackled. HISs prevent

propagation of surface EM waves in some frequency bands, called EM band gaps (EBGs). Immediate applications involve ground planes for adjacent antennas that prevent current circulation and therefore interaction between radiators and realization of artificial magnetic walls. Usually FSSs are planar, inhomogeneous structures, which bear a (quasi) periodic 2D pattern. The 2D period of the pattern is called unit cell. The interaction between FSSs and impinging EM waves gives rise to transmitted, reflected, and absorbed waves having various parameters changed with respect to the incident wave. This allows to control amplitude, phase, polarization, and direction of propagation of EM waves by appropriately shaping the unit cell, and to achieve wave focusing. Since FSSs can conduct surface waves outside EBGs, applications as absorbers have been devised. Reflectarrays and transmitarrays are special cases of non-uniform FSSs [6].

An important new research interest is directed to the realization of tunable and controllable FSSs. Control can be achieved by electrical means (using diodes or transistors), mechanical or optical means (by using photodiodes) etc. Dynamic control is a modern subject for research. Such solutions are applied to antenna beam steering by reflection or refraction, radiation pattern and side-lobe control in view of user tracking in 5G technology. Conformal FSSs have also been reported in the literature.

MSs are FSSs with sub-wavelength unit cells and sub-wavelength thickness that can be described by effective parameters, that can be either surface susceptibilities [5] or surface impedances [6]. MSs are designed to control far-field parameters of waves such as amplitude, phase, direction of propagation and polarization by means of impressed or induced electric and magnetic surface currents, based on the Love-Scelkunoff equivalence principle [7].

This chapter is meant as an introduction to the topic of applications of planar periodic structures etched on PCBs to support wave propagation and coverage. Solutions based on such structures embedded in the design of antennas are covered in other chapters of this book.

2 High Impedance Surfaces

High impedance surfaces (HISs) are 2D periodic structures implemented on PCBs that have been inspired from the predating concept of metamaterials. Metamaterials are artificial structures devised to interact with the EM field similarly to natural homogeneous materials (crystals).

An EM wave of a given frequency that propagates in the interior of a crystal is diffracted by the atoms or molecules situated at the points of the crystal lattice. If the wavelength is of the order of magnitude of the lattice spatial period, the scattered waves interfere constructively or destructively to give rise to secondary waves that propagate in some preferential directions. This phenomenon happens e.g., when a crystal is illuminated with X rays.

However, if the wavelength is much greater than the lattice constant, then waves scattered in adjacent points of the lattice have a negligible phase differ-

ence and consequently add in phase. This is the common case of a plane wave propagating through a homogeneous medium and not changing the direction of propagation.

The incidence of a plane wave on the separation surface between two homogeneous media is described by the laws of Snellius-Descartes and Fresnel coefficients. From an EM point of view, media are characterized by constitutive parameters ε (permittivity) and μ (permeability), which can be scalars or tensors, or may describe nonlinear materials. The constitutive parameters are complex functions of frequency in general. The imaginary part of the permittivity accounts for dielectric and conduction losses (including conductivity in the last case) and the imaginary part of the permeability accounts for losses of magnetic origin. The real and imaginary parts of both constitutive parameters are inter-related due to causality constraints.

A limited range of values for constitutive parameters can be found in homogeneous natural materials, albeit isotropic or anisotropic. Wave propagation is affected by dielectric, magnetic or conductive losses. Metamaterials propose a solution to this issue (among other applications). Media with simultaneously negative permittivity and permeability have been reported as a breakthrough [8, 9], with spectacular applications, such as flat lenses and negative refraction [10]. Cloaking at microwave frequencies have been also proposed as potential applications of metamaterials [11]. Another relevant example consists of the conception of HISs and, implicitly, of magnetic walls (Artificial Magnetic Conductors – AMCs). The boundary conditions at the interface of a common material and an AMC are dual with respect to those found at the interface with an electric wall (Perfect Electric Conductor – PEC). Both media with negative constitutive parameters and AMCs have not been discovered in nature.

An important category of metamaterials originates from periodic structures, which can be 1D, 2D, or 3D. To operate like a metamaterial, it is necessary that the spatial period(s) of the structure be much smaller than the wavelength of the EM radiation with which it interacts. If this is not the case, the structure behaves like a photonic crystal. However, in practice it is accepted that the period extends up to a quarter wavelength [12]. Metamaterials can be realized as random spatial structures or fractal structures too.

The propagation of EM waves through periodic structures presents similarities with the propagation of electronic waves through crystals. For example, EM (frequency) bandgaps (EBGs) exist, where propagation phenomena cannot take place and waves are evanescent (or leaky in the case of open structures). Propagation occurs in complementary frequency bands. However, this filtering property of the periodic structures has been known for quite a long time in microwaves applications, before the occurrence of the concept of metamaterial, and it has been used e.g., in filter design.

The propagation of EM waves in periodic structures is described by the Bloch-Floquet theorem. The intensity of the monochromatic electric field can be written as a product between a periodic function and a propagation factor. Expanding the periodic function in a Fourier series in the dual space of

wavenumbers, the spatial harmonics, also called Bloch harmonics are obtained. The presence of the propagation factor determines that the values of the field distanced by one period (also called unit cell) to be different only by a phase factor that depends on the wavenumber. This has important implications in the numerical calculation of the field by introducing so-called Periodic Boundary Conditions, and the corresponding ports are called Floquet ports. It is worth mentioning that spatial harmonics share the same group velocity but have different phase velocities, and the directions of the two may be different. In particular, the phase and group velocities might have opposite directions (also a fact known and applied for a long time in Microwaves).

The graphical representation of the dispersion law of the periodic medium, i.e., of frequency vs. (normalized) wavenumber, is called dispersion diagram (DD). The DD is periodic, of period 2π in the normalized case, over every axis in the wavenumber space and it allows for quick identification of EBGs and for calculation of phase and group velocities. Brillouin zones are relevant for DDs. In the 2D case, the DD is a 3D representation that can be reduced to a 2D one by considering the first irreducible Brillouin zone (spectral triangle $\Gamma XM\Gamma$ an example will be given below) [13].

The scientific interest in metamaterials shifted from bulky 3D to more feasible 2D structures in the last years. A common practice is to etch a periodic pattern on one or both sides of a PCB, which, depending on the application, can be of high quality or a cost effective one such as FR4. One or several vias can connect the metallic pattern on one side to the patterns or ground plane on the other side of the PCB. The 2D versions of metamaterials are called metasurfaces. Homogenization of parameters shifted from the 3D effective permittivity and permeability to effective surface susceptibilities or to an equivalent surface impedance formulation. The structure can be completed with active elements, diodes, or transistors to allow for switching its wave processing properties in a way fit for various applications.

Metasurfaces relate to general 2D periodic structures in the same way metamaterials relate to photonic crystals: the spatial periods being much smaller than wavelength, effective parameters can be defined and used in theoretical analysis. When the wavelength related condition is not met, or when effective parameters are not of interest in the considered application, 2D periodic structures are called Frequency Selective Surfaces (FSSs) in the Microwaves literature. The name indicates that the type of response of the surface changes with frequency, due to the dispersion law.

The amount of literature dedicated to the topic of this chapter is huge. Therefore, we have limited the number of references, and illustration of introduced ideas is made mainly through authors' own work. However, additional information and other illustrations can be found in scientific and engineering publications.

The interest in engineering applications of 2D periodic structures has been raised by the seminal publication [14]. Sievenpiper's "mushroom" structure consists of an array of rectangular metal patches separated from the ground plane

by a dielectric and connected to it by vias, Fig. 1 (a-c). A surface impedance has been associated to the planar structure by analogy to the approximate boundary conditions at the interface between a metal of conductivity σ and a dielectric.

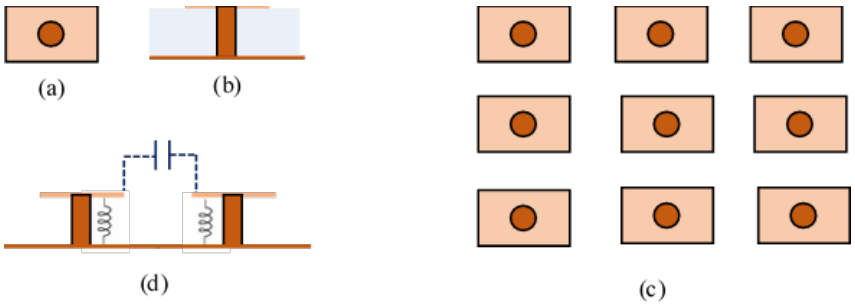

Fig. 1. Sievenpiper's "mushroom" structure: (a) unit cell top view; (b) unit cell side view; (c) periodic surface obtained by the repetition of the unit cell; (d) simple, approximate circuit model.

It is known that, at the metal-dielectric interface subject to a plane wave incidence from the dielectric side, the tangential electric field vector is perpendicular to the tangential magnetic field vector and the two are related by an impedance approximately equal to the plane wave impedance in the metal (the wave in the metal propagates approximately normally to the interface regardless of the angle of incidence).

For the mushroom structure, the surface impedance has been considered in a first approximation to originate from L-C elements determined by the inductivity of the vias and the capacitance between adjacent patches. At resonance, the impedance becomes very high and surface waves (also called plasmons) are prohibited to propagate, therefore the name of HIS. The presence of the EBG is confirmed by the numerical calculation of the DD and experimentally.

Later, more exact design procedures for Sievenpiper's HIS have been devised [15].

Some immediate applications of HISs are to leaky wave generation [16], Fig. 2 (a), antenna grounds Fig. 2 (b) and AMCs. The operation of leaky wave antennas is based on the existence of fast surface waves (plasmons). The continuity of the wave vector at the interface with the surrounding space requires that a part of the plasmon be radiated in a direction in space that can be controlled through the plasmonic wavenumbers, statically or dynamically, so that antennas with prescribed radiation patterns can be designed. Leaky wave antennas are treated in another chapter of this volume.

Antennas sharing a common metallic ground plane interact in near field and exchange currents through the ground with unfavorable consequences for their gains and radiation patterns. The currents reaching the bounds of the ground

plane (which must be of finite size for feasibility reasons) radiate, generating speckle in the radiation patterns. To prevent exchange of currents, a periodic pattern can be stacked over the ground plane (Fig. 2 (c)), having an EBG in the operation bands of the antennas [14]. This solution is incorporated quite often in the design of modern, compact, low-profile antenna arrays realized on microstrip boards.

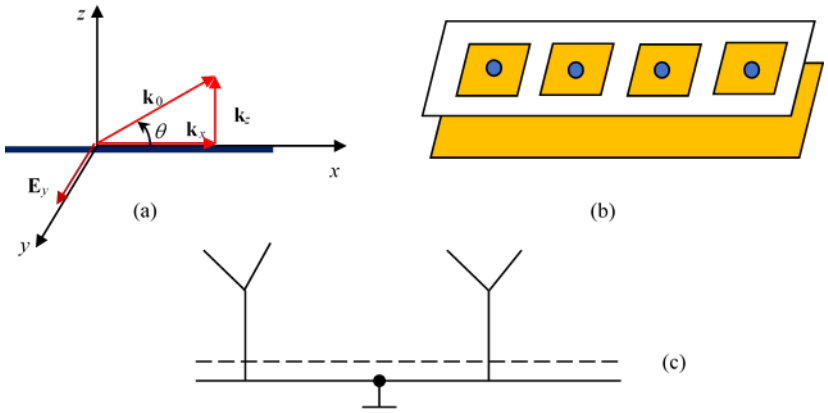

Fig. 2. Application of surface waves: (a) fast waves at the interface of a periodic structure and free space (wavenumber k_0) used in leaky wave antennas; (b) periodic structure for leaky wave antenna (the structure must be completed with matching and feeding elements); (c) antennas sharing a common ground plane with EBG periodic structure added to obstruct propagation of surface waves.

An EBG structure functions like an AMC in the frequency range of the EBG due to its high impedance. As well known, at the interface between a PEC and a dielectric, the tangent component of the electric field is zero. This has many consequences, e.g., the radiation of an antenna placed near an electric wall is cancelled by its electrical image. To have a constructive interference in a plane perpendicular to the antenna, it must be placed at a quarter wavelength distance from the wall Fig. 3 (a). In the case of a magnetic wall, it can be shown that the image of the dipole is not inverted, so that the antenna can function in the immediate proximity of the wall, Fig. 3 (b) [14].

Other applications of HIS involve parallel plate noise (PPN) filtering and cavity oscillation modes suppression.

Multilayered PCBs usually have an inner metallic power supply layer parallel to a ground layer, Fig. 4 (a). The two planes are pierced by vias with metallic walls that connect traces from different signal planes. Since vias sustain currents with fast time variation, EM waves radiation occurs, which propagate as a noise in the parallel-plate waveguide (PPW) formed in between the power supply and ground planes. These waves have a power density spectrum that is quite flat

up to several GHz (6 GHz is a commonly used limit, note the coincidence with the 5G band), resemble a low pass filtered white noise, and form the PPN (also called "Ground Bounce Noise" due to ground potential jumps).

Propagation of the PPN can be obstructed or attenuated by mounting a HIS periodic structure over the ground plane, Fig. 4 (b). The noise is eliminated in the frequency range of the EBG of the periodic structure [17–19]. In this way, a new type of PPW has been introduced, with one of the two electric walls replaced by a magnetic one, since the periodic structure behaves like an AMC in the frequency range of the EBG.

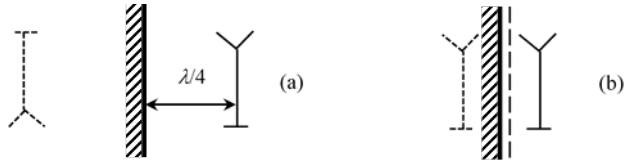

Fig. 3. Magnetic wall: (a) antenna placed in front of an electric wall to obtain a constructive interference in far field, and electrical image; (b) similar configuration but with magnetic wall.

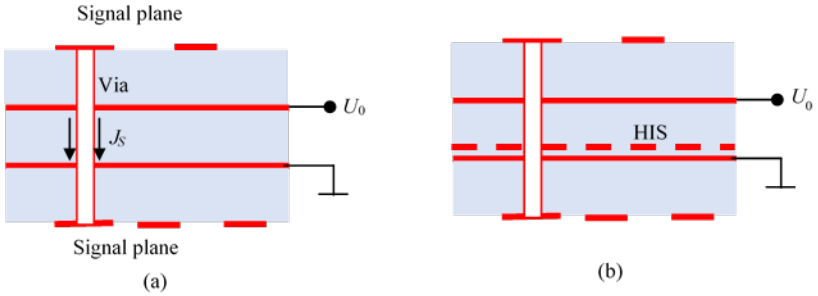

Fig. 4. Multilayered PCB: (a) initial design; (b) HIS inserted for PPN reduction.

Often electronic circuits are screened from the environment to avoid EM interaction by inclusion in closed metal boxes, Fig. 5 (a). The method is effective, but it presents the drawback of possibly introducing perturbations to the normal operation of the screened circuit caused by cavity mode oscillations that can be launched inside the box, which constitutes a resonant cavity, sometimes with a high Q. The traditional solution to avoid oscillations is to artificially increase damping by introducing resistive materials inside the box [20]. However, this solution also introduces energy losses for the power supply by Joule effect and

therefore the efficiency of the system is diminished. A better solution relies on introducing an EBG periodic structure inside the box [21, 22], Fig. 5 (b).

Fig. 5. Metal box screening a grounded circuit: (a) initial design; (b) improved design with insertion of a HIS.

The EBG of the inserted periodic structure must include the operational frequency band of the screened circuit. In this case, one of the walls of the box acts like an AMC and the boundary conditions at this wall will prevent launching of cavity oscillation modes. Consequently, the screened circuit will operate unperturbed and with negligible spurious energy losses.

To demonstrate the flexibility in the design of periodic structures realized on PCBs allowed by the possibility to vary the geometry of the metallic patches, consider the example illustrated in Fig. 6, consisting of a periodic pattern sandwiched between two dielectric layers covered with metallic planes (which can also be viewed as a PPW filled with dielectrics and the pattern plane, or as a multilayered PCB) [23]. The unit cell is square shaped, with a side of 2.5 mm, which also plays the role of spatial period, Fig. 6 (a). The relevant dimensions of the metal pattern are given in the cited reference. The CAD model of the unit cell is reproduced in Fig. 6 (b) (the upper metal plane has been removed for providing visibility of the structure). Three vias with metallic walls, of radius 0.1 mm, connect the pattern to the ground plane. The dielectric inserted between the periodic pattern and the ground, distanced by 1.6 mm, has a dielectric constant of 3.5. The upper metal plane is separated by a layer of thickness 0.16 mm from the pattern plane.

The DD in the 2D wavenumber space rendered in Fig. 6 (c) for the first five propagation modes features the remarkable fact that a quite large EBG is present between every two consecutive modes. To obtain such a behavior, the dielectric in the upper part of the unit cell must have a large dielectric constant, 30 in this case. Contemporary progress in devising dielectric materials allow for such values of the dielectric constant. The meander shape of the metallic pattern and the three vias ensure a sufficient number of separate resonances to obtain the described behavior of the periodic structure. Increasing complexity of the design requirements determine the increase of the complexity of the metal patch in general.

Another interesting feature revealed by Fig. 6 (c) is the relation between the 3D DD and the DD reduced to the boundaries of the first Brillouin irreducible zone $\Gamma XM\Gamma$ highlighted in the wavenumbers plane and its image on the modes surfaces). Note that the restriction of the DD to the spectral triangle, which can

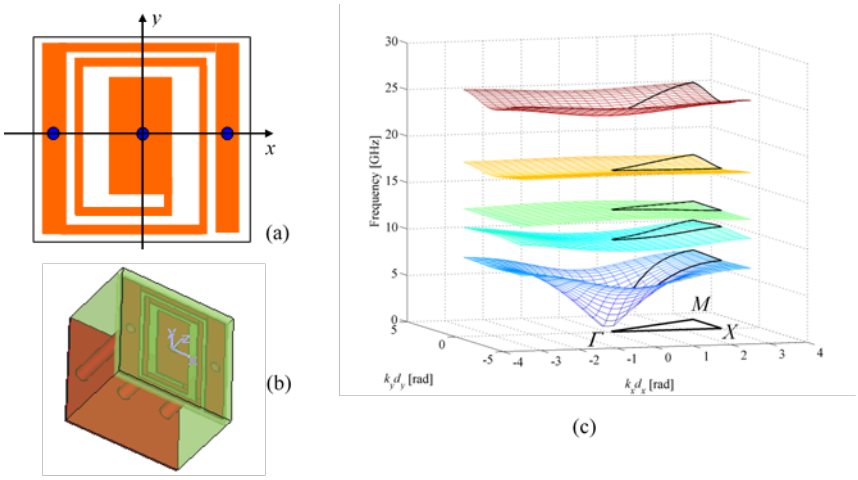

Fig. 6. Periodic structure in inhomogeneous PPW featuring EBG between every two consecutive modes of the first five modes. (a) Metallic patch and vias; (b) CAD model of the unit cell (upper metal plane removed for a better rendering); (c) DD with the Brillouin spectral triangle highlighted. (Adapted from [23].)

be represented as a 2D graph, provides a relevant perspective on the complete 3D DD, and requires a smaller consumption of computation time and computer resources.

The proposed structure can be used for filtering, e.g., in antenna feeders. Furthermore, the higher order modes in Fig. 6 (c) are resonant (flat), i.e., cover a small interval on the frequency axis. Such modes are fit for sensor applications.

The metamaterial counterpart of the structure is restricted to large wavelength (small frequencies).

The fixed periodic structures presented so far are based on unit cells with given geometry and materials, which determine the EM behavior of the structure. By adding switching devices, like diodes or transistors, periodic structures with switched geometry can be devised. However, one of the most critical issues to be solved in this case is the design of the biasing network necessary to control the active devices (in this context, a device is considered active if it needs a power supply for normal operation). Because of its metal composition and spatial extension, the biasing network can greatly influence the response of the structure to incident EM field [24]. In fact, from a design point of view, it is recommended to consider the biasing network as a part of the structure.

As an example, consider the design in Fig. 7, consisting of an inhomogeneous PPW with switched geometry devised for filtering applications [25]. The metal pattern of the periodic structure (Fig. 7 (a)) consists of an elliptical patch connected to the ground plane through two vias. The pattern is a variation of the "mushroom" structure presented above, but the elliptical form of the patch has been chosen to provide a "smoother" path for the surface current and two vias

instead of one change the equivalent inductance. Furthermore, displacing vias from the center of the patch gives further degrees of freedom in tailoring the DD according to design requirements [26]. A metallic pin, connecting the patch to the upper plane of the PPW has been added and two slots around have been etched to allow the placement of the diodes D1 and D2. The diodes are biased through the metal planes of the PPW, avoiding in this way the need for biasing lines or wires. The diodes can be mounted in opposition, as in Fig. 7 (a), in which case only one of them is in conduction when the bias is applied between the two metal planes, or they can be mounted in series, in which case the metal planes are in a short-circuit. This is an interesting situation, since the short-circuit in dc obstructs waves from propagating through the waveguide at low frequencies, introducing in this way an EBG starting from zero frequency.

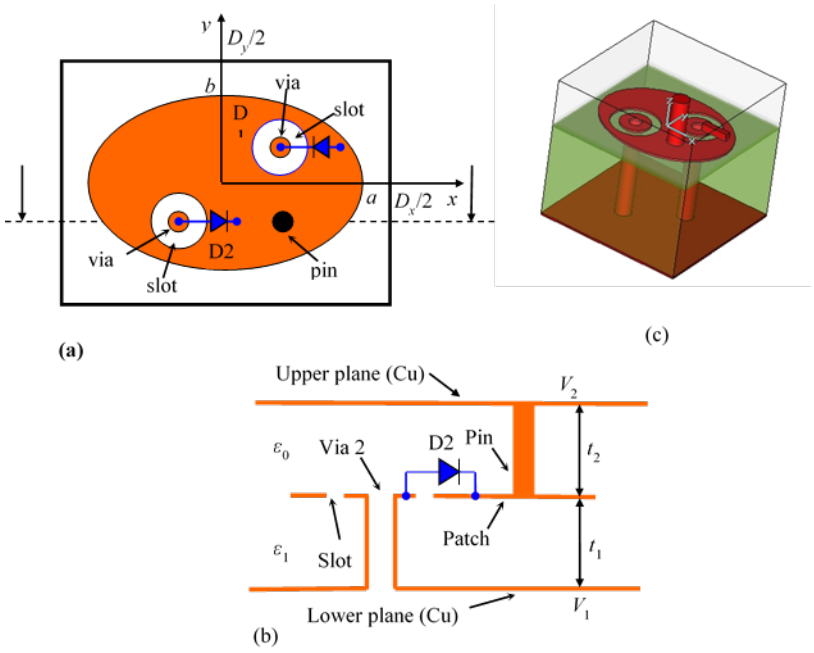

Fig. 7. Unit cell of a periodic structure with switched geometry. (a) Elliptical patch with two vias and pin; (b) cross-section through the unit cell, D2 in conduction; (c) CAD unit of the unit cell in a PPW, with D2 in conduction (upper metal plane removed for visibility reasons) [25].

The CAD model of the square shaped unit cell is reported in Fig. 7 (c). The sides have a common length of 2.5 mm, the space between the patch and the ground, of height 1.6 mm is filled with a dielectric material having a dielectric constant of 3.5, and the space above the patch, of height 0.8 mm is free (filled with air). The exact design is given in the cited reference. In the simulation, a

diode in conduction has been replaced by a small metallic parallelepiped (Fig. 7 (c)) and a blocked diode by an empty space. This gives insight into the possibility to switch the geometry by using diodes.

Suppose the two metal planes that bound the PPW are at different potentials: the ground at potential V1 and the upper metal plane at potential V2. If V1<V2, the diode D1 is in conduction and D2 (Fig. 7 (a)) is blocked. The converse holds when V1>V2. If V1=V2, both diodes are unbiased. The DDs calculated on the sides of the Brillouin spectral triangle are represented in Fig. 8 (first five propagation modes) as follows: both diodes unbiased in Fig. 8 (a) and D1 in conduction and D2 blocked in Fig. 8 (b). As mentioned, one of the diodes can be reversed so that both diodes can be either in conduction or blocked. The DD corresponding to the case of both diodes in conduction is represented in Fig. 8 (c).

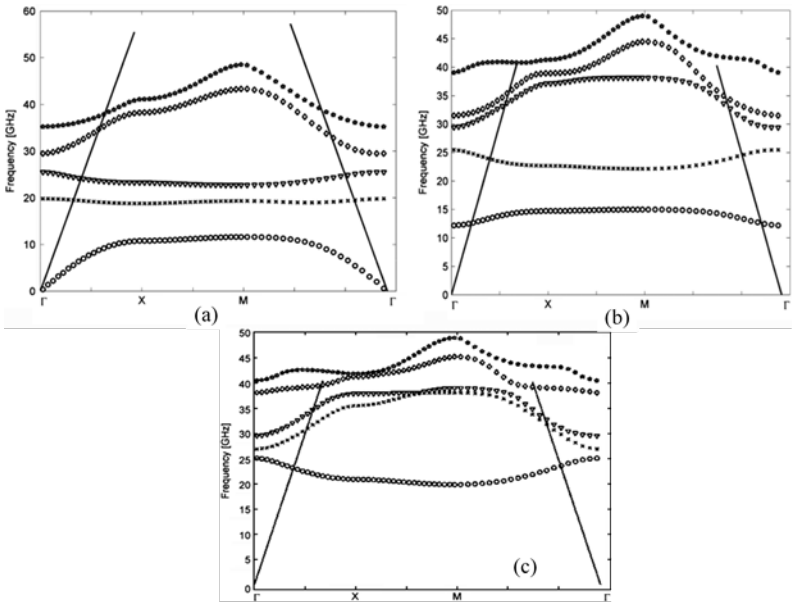

Fig. 8. DDs corresponding to the switched structure, the first five modes: (a) both diodes blocked; (b) D1 in conduction, D2 blocked; (c) both diodes in conduction. Light lines are also drawn (for a bulk, effective medium) [25].

Figure 8 reveals that the band structure of the device can be controlled by electronic means. DD in Fig. 8 (a) corresponds to a low-pass filter in low frequency and displays a resonant behavior between 20 and 30 GHz. After switching D1 to conduction, a high-pass filter is obtained (Fig. 8 (b)) and the resonant mode around 20 GHz vanishes. When both diodes are biased, the obtained DD

(Fig. 8 (c)) has a high-pass pattern, but the stopband is larger than in the case corresponding to Fig. 8 (b) and higher order modes are not resonant.

In conclusion, periodic structures, and consequently metamaterials, can be realized as switched geometry devices by periodic insertion of electronic devices, like diodes or transistors. The necessity of a biasing network has an important impact on the way the structure interacts with EM waves. In some situations, this impact can be mitigated by using the metallic elements of the structure for applying the biasing voltage.

In this paragraph, some applications of periodic structures that conduct surface waves (plasmons) have been presented. Other applications are concerned with the interaction of periodic structures with incident plane waves. This will be the subject of the next paragraph.

3 Frequency Selective Surfaces and Metasurfaces

Frequency Selective Surfaces are periodic arrangements of identical or similar elements disposed in a plane. In a large majority of cases, the elements are metallic or dielectric resonators and the main useful properties of FSSs occur at or around the resonance frequencies of the elements in general.

To fabricate an infinitely thin (2D) FSS according to the definition is a technological impossibility. For this reason, the surface is realized on a substrate of a certain thickness, such as the dielectric of a PCB or a film. This gives rise to many developments, such as cascading FSSs by etching both sides of a single layer PCB or cascading several FSSs by using multilayer PCBs or even separating several PCBs by air layers. By extension, these solutions are also called FSSs, or even 2.5D FSSs when the extension in the transversal direction is important. In many situations, e.g., for creating magnetic current flow in metasurfaces, it is critically important to place loop resonators in the space between the metallic patterned layers.

The main applications of FSSs are in relation to the response to incident plane waves. Like for a diffraction grating, reflection and transmission in several directions can take place (lobes) and a surface wave (plasmon) can occur. The possibility to divert EM radiation in several directions can be used to develop antennas diversity. Furthermore, FSSs with switched or controlled geometry can be used for dynamic change of the radiation pattern or for user tracking without resorting to more complicated and bulky electronic circuits for phased arrays control.

Knowing the number of lobes produced by a plane wave that is incident on an FSS coming from a given direction is important. Although FSSs are 2D structures, an insight is gained by considering the 1D situation in Fig. 9 [27].

The period of the structure is denoted by Λ and let λ denote the wavelength in Fig. 9 (a). By considering the path difference for both reflected and transmitted waves, the condition of phase matching at the boundary reads:

$$\frac{2\pi}{\lambda}\Lambda(\sin\phi + \sin\theta) = 2n\pi, n : \text{integer} \tag{1}$$

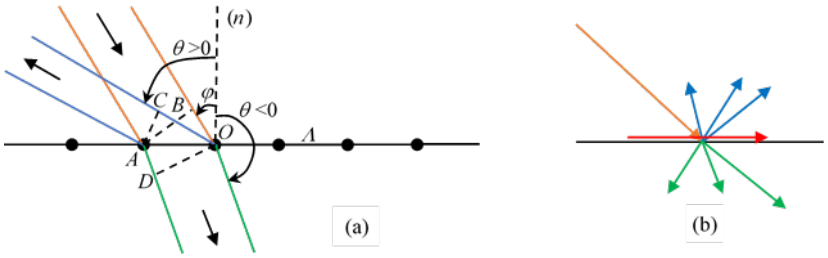

Fig. 9. Plane wave incident on a 1D periodic structure: (a) phase matching; (b) reflected, transmitted and surface waves.

Note that this condition is fulfilled for specular reflection ($\theta = -\phi$) and for direct transmission ($\theta = \phi - \pi$) $n = 0$. Also note that (1) implies

$$|n| \leq \frac{\Lambda}{\lambda}. \tag{2}$$

Therefore, when the wavelength is (much) greater than the dimension of the unit cell, only the reflected and the directly transmitted waves are propagative. No secondary lobes occur in this case. Otherwise, reflected, transmitted and surface waves can be launched, as suggested in Fig. 9 (b). The angle θ depends on frequency.

FSSs are planar structures in general. However, properties derived or measured for planar surfaces can be applied to surfaces with large curvature radii by replacing the surface with the tangent plane at the point of interest [28]. With this in mind, Fig. 10 suggests some applications of FSSs to enhancing antenna diversity, screening, filtering and radomes.

In Fig. 10 (a), FSSs are used as wallpapers to shield a space against one or more communication signals such as GSM or LTE (or 5G in the future), allowing signals from other frequency bands to pass (approximately) undisturbed. Classical applications exist to conceptions of radomes in the radar technology, Fig. 10 (b), to protect airborne vehicles from radars operating of various frequencies by scattering or reflecting at certain angles incoming radiation (RCS reduction) and allowing at the same time communications through the in-built antenna [27]. Another well-known application consists of allowing an antenna to work simultaneously at two or more frequencies by redirecting radiation to spatially separate feeding horns (dichroic reflectors, Fig. 10 (c)). In Fig. 10 (d), the antenna beam is redirected to some targeted spots by the FSS, or it is spread in a certain space to enhance coverage [2]. If the FSS is active and controlled by some means (electronically, optically, mechanically etc.), dynamic redirection or user tracking can be achieved. Other applications such as thin lenses, polarization processing and conversion and spatial filtering can be found [4, 29]

Several simple metal patterns imprinted on the unit cell that have been used in various applications are presented in Fig. 11 (a)-(e) [30], [28], [31]. Such structures are resonant and present a band-stop frequency response in transmission,

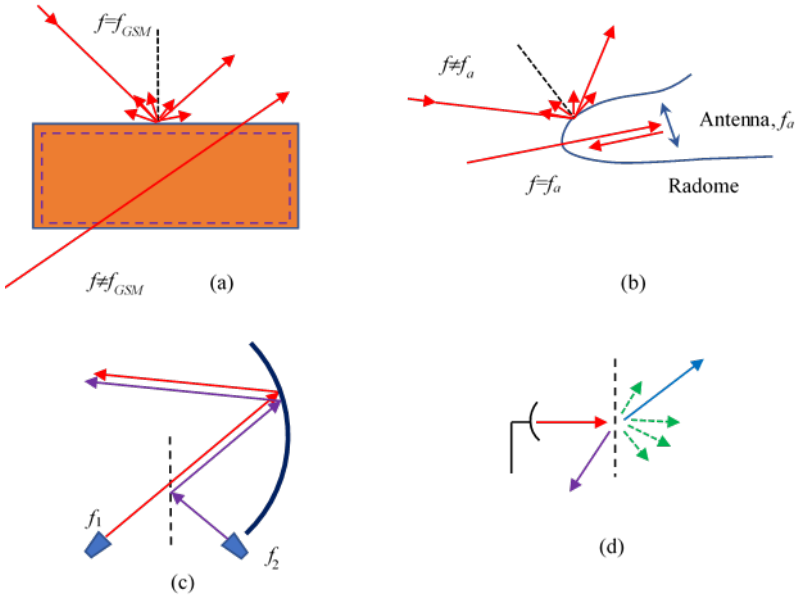

Fig. 10. FSS applications: (a) Screened space at some frequencies (b) radome; (c) dichroic reflector (d) redirection of antenna radiation by reflection and/or transmission at different angles or diffraction.

in general, like in Fig. 12 (a). The "negative" of the patterns can also be considered Fig. 12 (b), which present a band-pass frequency response in transmission, Fig. 12 (b). The Babinet theorem might be invoked to explain this situation, however this is only an approximation since the medium at the back of the metallization is not homogeneous, a dielectric layer being necessary to support the pattern [28].

The metallic pattern can be replicated on the other side of the board or two different patterns can be combined to enhance the filtering properties in transmission, Figg. 11 (f) and (g) [27]. The space in the dielectric in between the metallic patterns is used sometimes as a Fabry-Pèrot resonator. To increase the number of resonances, fractal patterns are considered, Fig. 11 (h), or fractals in combination with simple resonators such as the cross dipole, Fig. 11 (g).

To choose a model for the FSS, the relation between the unit cell dimension and wavelength bears a crucial importance [5], [31]. For very large wavelengths, the FSS behaves like a homogeneous material and can be treated by constant material parameters. For wavelength greater than the dimension of the unit cell, but of the same order of magnitude (see e.g., (2) for a 1D analogy), there are still one transmitted and one reflected wave, but the parameters of the structure depend on the direction of incidence and polarization of the incident wave. It is considered that the surface exhibits spatial dispersion [6]. For smaller wave-

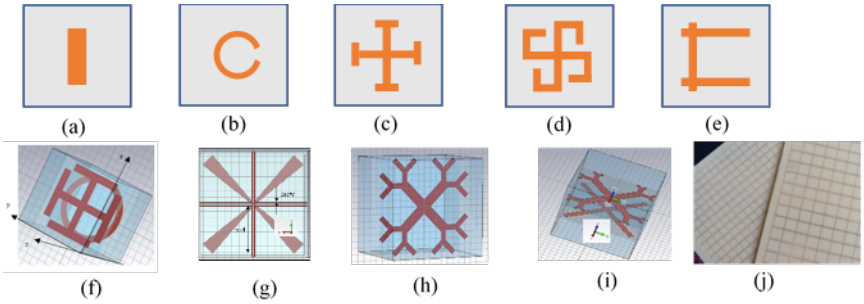

Fig. 11. Metallic patterns of the unit cell for FSSs: (a) dipole; (b) split ring resonator; (c) Jerusalem cross; (d) square spiral; (e) U-shaped; (f) Jerusalem cross combined with circular resonator; (g) "fan" shape combined with displaced cross dipole; (h) fractal; (i) fractal combined with cross dipole (the last four images are CAD models); (j) PCB implementations of FSSs based on the U-shaped unit cell.

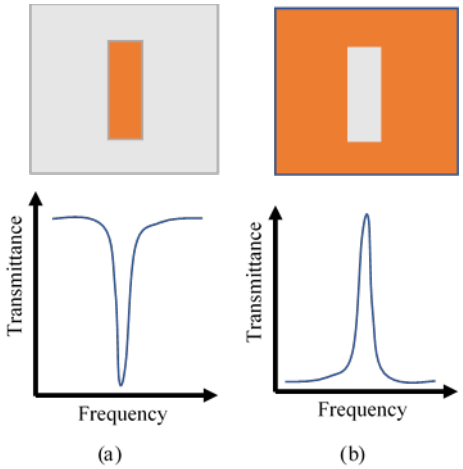

Fig. 12. Complementary patterns: (a) band-stop; (b) band-pass.

lengths, Bloch harmonics of the surface wave and a multimode approach must be considered. An in-depth treatment of this topic can be found in [31].

The response of the FSS to an incident plane wave depends on the polarization of the wave in general, which can be TE (the **E** vector parallel with the plane of the FSS) or TM (the **H** vector parallel to the plane of the FSS). When the FSS is used as a screen or as a spatial filter [32], the two responses must be made as similar as possible. This can be achieved with patterns exhibiting a high degree of symmetry, like those in Figg. 11 (c) and (f)-(i). When the targeted application requires an anisotropic response, e.g., for polarization filtering or conversion, non-symmetric patterns like in Fig. 11 (e) must be used.

As a further opportunity offered by the planar configuration, is that it also well adopts to implement configurations of higher order symmetries, such as glide symmetry [33]. Rotation and translations of the initial pattern will not require neither additional space, since this mirrored pattern is still planar nor will increase the fabrication cost, since the same technology can be applied. Such configurations exhibit a wider bandwidth that can be efficiently exploited in applications requiring huge data throughput, i.e., 5G and 6G.

As an example of the transmittance (magnitude of the transmission coefficient) of a FSS, consider the graphs in Fig. 13, which correspond to the FSS based on the unit cell in Fig. 11 (g) [34], working in the sub-6 GHz band, which presents interest for future 5G applications. The structure has been intended to operate as a filter with two notches. The transmittance vs. frequency in TM incidence for several values of the incidence angle is represented in Fig. 13 (a) (showing a small dependency in this case, which is a desirable feature for a filter). In Fig. 13 (b), the transmittance vs frequency in TE normal incidence for several values of one of the geometrical parameters shows that one of the notch frequencies can be fixed by varying this parameter, while the other one remains (quasi) constant.

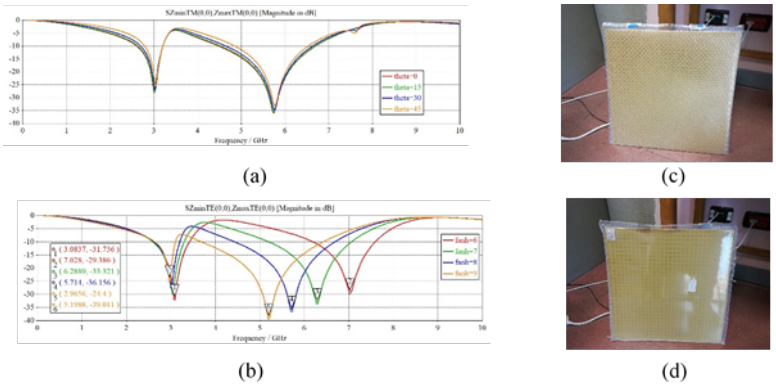

Fig. 13. Transmission coefficients for the structure in Fig. 11 (g) with a size of the unit cell of 15 mm: (a) for various angles of incidence (TM case); (b) for various sizes of the "fan wings" (mm) (TE incidence). (c) Side of the PCB with the "fan" pattern; (d) Side of the PCB with square rings pattern.

The response of a FSS to an incident plane wave can be understood in terms of a circuit model, Fig. 14 (a). The generator e_g with internal impedance Z_0 equal to the wave impedance of the surrounding medium accounts for the incident wave. The two-port simulates the metal pattern, and the transmission line accounts for the propagation through the dielectric layer that supports the metallization. The circuit is terminated on the impedance of the medium Z_0. The length t of the transmission line is equal to the thickness of the dielectric substrate,

the characteristic impedance Z_ε and the propagation constant β are equal to the wave impedance and wavenumber of the dielectric material, respectively. The equivalent circuit parameters depend on the direction of arrival (spatial dispersion) and polarization of the incident wave. The two-port is passive and lossless in general. However, if losses must be considered, dissipative elements must be added.

In many situations, the two-port involves a simple impedance in derivation, Fig. 14 (b). For example, the equivalent circuit for the FSS with the transmittance in Fig. 13 (a) is composed of two series LC circuits connected in parallel, which account for the two notches. A similar model holds for the FSS based on the Jerusalem cross [31].

A simple example of circuital model dependent on polarization is related to the dipole in Fig. 11 (a), which resonates when the **E** field of the incident wave is parallel to the dipole and the length is approximately equal to one half wavelength. In this case, the character of the dipole is slightly inductive. When the **E** field is perpendicular to the dipole, the equivalent circuit has a capacitive character [27].

Finding the equivalent circuit for an FSS involves decomposing the structure into simple elements that interact, based on field images, and applying low-frequency formulas for finding capacitances, inductances, and resistances if appropriate [31], [35]. In most cases, the calculated values for the parameters are only approximately satisfactory, so that an optimization process is needed to obtain coincidence between the transmission coefficient and the S_{21} parameter of the model. For example, the inductance L of the dipole of Fig. 11 (a) of length s and width w, situated in a non-magnetic material, is given by the following formula, valid for the case of a negligible thickness [36]:

$$L = \mu_0 \frac{s}{2\pi} \ln \frac{2s}{w} \tag{3}$$

However, applying this formula gives an approximate result, mainly because the current density is only approximately constant through the extension of the dipole in the situation when the FSS exhibits spatial dispersion. Other useful formulas for equivalent lumped elements associated to various geometrical configurations can be found in the literature.

In the case of multilayer (stacked) FSSs, circuital models involve a cascade of systems like the one in Fig. 14 (a), accounting for the dielectric layers, the metallic patterns and possibly the interactions between them.

FSS-based spatial filters intended for working in the 5G mm-wave range have already been reported in literature. A solution with three metallic layers separated by two dielectric layers of 0.07 λ thickness, operating as a band-pass filter at 27.5 GHz, with a relative -3 dB bandwidth of 20.5% has been proposed in [37]. The upper and lower layers contain circular rings, and the middle layer has a more complex etched pattern, surrounded by an etched square ring slot, to ensure a greater roll-off at the bounds of the passband. The dimension of the unit cell, having the shape of a square, is 6.2 mm (0.57 λ). A complex circuital model has been proposed and compared against simulation and measurement

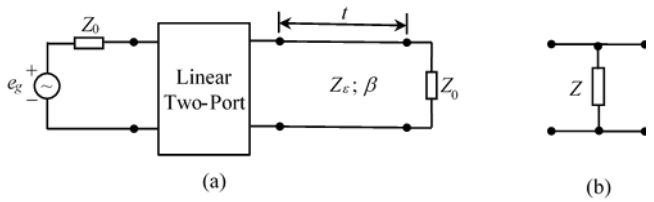

Fig. 14. Equivalent circuit for a FSS in transmission: (a) general schematic; (b) simplest structure of the two-port.

data. The structure has been experimentally tested up to an incidence angle of 40° (the structure is insensitive to polarization due to the symmetrical shape of the metal pattern in the unit cell).

Another solution, consisting of a unit cell having the side of 2.27 mm and an upper part with a metal pattern composed of a meandered line surrounded by a square ring, and 12 vias having a height of 0.38 mm has been reported [36]. The lower part is the mirror image of the upper part and the two are separated by an air foam. The structure has a pass-band type transmittance centered at 28 GHz with a 2 GHz -1 dB bandwidth and two notches at 32 GHz and 38.5 GHz. A circuital model has been proposed and assessed. Consistent simulation and measurement results indicating proper operation have been obtained up to a 60° angle of incidence.

A 5G EM shield with ventilation holes has been proposed in [38]. The periodic structure, with a spatial period of 4.91 mm in two orthogonal directions, has been implemented on a cost-effective FR4 substrate, having a thickness of 2.5 mm. The metallic pattern consisted of a slotted circular ring, split into four parts, and replicated on the other side of the board. A ventilation hole, having a radius of 2 mm has been drilled at the center of the unit cell. The shield has been proved to work at 28 GHz with at least 30 dB shielding effectiveness in a 2 GHz wide band around the center frequency and with proper operation up to a 60° angle of incidence.

Many tunable solutions for FSS-based spatial filters have been reported, see e.g., [39] for a mechanically reconfigurable FSS.

Spatial filters used for screening and shielding have a symmetric pattern imprinted on the unit cell to ensure polarization insensitivity. When polarization processing is involved, the pattern cannot be symmetrical anymore. For illustration, consider the U-shaped pattern in Fig. 11 (e), which can be used as a linear polarizer. For a unit cell dimension of 12 mm, the transmission coefficient for incidence with the **E** vector parallel to the single dipole has a notch at 2.88 GHz, with a transmittance of -29.88 dB, and for the incidence with the **E** vector parallel to the pair of dipoles, a notch occurs at 6.6 GHz, with an attenuation of -28.80 GHz. The attenuation at the notch frequencies of the polarizations in the case of the orthogonal polarizations are -0.98 dB and -2.03 dB respectively [40].

However, a more interesting application of FSSs to polarization processing is the linear-to-circular polarization conversion. This application has a favorable impact on antenna design requirements since linearly polarized antennas can be more conveniently devised than circularly polarized ones. The interest in circularly polarized waves stems from the smaller sensitivity to propagation effects such as fading, reflections, polarization plane rotation (Faraday effect) etc. than the linearly polarized counterparts.

A simple approach to polarization conversion consists of considering an asymmetric pattern of the unit cell, thus having different transmission coefficients for $x-$ and $y-$polarized waves respectively, Fig. 15.

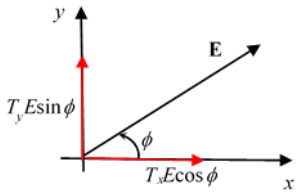

Fig. 15. Linear to circular polarization conversion.

Consider a linearly polarized wave propagating in the negative direction of the z axis, with the **E** vector making an angle ϕ with the x axis, which is incident on the FSS situated in the xOy plane. Let T_x and T_y denote the transmittances for $x-$ and $y-$polarized waves when the phase difference between the transmission coefficients is $\pm 90°$. Then the outgoing wave will be circularly polarized if

$$\tan\phi = \frac{T_x}{T_y} \tag{4}$$

If the phase difference between the y and x transmitted components of the E-field is $+90°$, the outgoing wave is right circularly polarized, and it is left circularly polarized if the phase difference is $-90°$.

Many publications that rely on this idea to devise polarization converters consider the case when $\phi = \pm 45°$ so that $T_x = T_y$ when the phase difference between the transmission coefficients is $\pm 90°$.

There are several parameters to be considered to assess the performance of linear-to-circular converters. One of these parameters is the insertion loss at the conversion frequency, which must be smaller than 3 dB. Losses occur from reflection and absorption of part of the energy of the incident wave. Other parameters are related to the quality of the circularity of the transmitted wave when deviations from the ideal circular form are present. The outgoing wave is elliptically polarized in general. The axial ratio AR is the ratio of the major half-axis to the minor half-axis of the polarization ellipse. For a circular wave, the AR is 1. The AR frequency band of the polarizer is the frequency band in

which the axial ratio at the output is below 3 dB (a widely accepted value) in normal incidence.

The performance assessment of the polarizer in oblique incidence must consider the asymmetry of the pattern in the unit cell. In general, both TE and TM incidences are tested for various colatitudes at azimuth equal to 0 and 90°. The angular stability of the polarizer is defined in terms of AR, the limit value being again 3 dB.

Many solutions have been reported in the literature using single or stacked FSSs. Single sided FSSs realized on PCBs have the advantage of convenient feasibility and cost-effectiveness. Multilayer solutions enhance desired properties of FSSs such as larger bandwidth and smaller insertion loss [27].

Many interesting solutions to the polarization conversion problem have been reported in the last years, some of them relevant for the 5G frequency range. The polarizer reported in [41] has an AR band between 18 and 20 GHz, an insertion loss smaller than 3 dB, and a proper response up to an angle of incidence of 30°, for a dimension of the unit cell of 2×3.5 mm. The metallization is a combination of a meander line and a loop. A dual band polarizer has been introduced in [42], based on a split ring and a closed square ring as metal pattern. The structure operates at 17.2 GHz and 34.2 GHz introducing opposite circular polarizations with 21% AR bandwidth and angular stability of 45° and 30° at the two central frequencies, respectively. The side of the square-shaped unit cell has been of 5.2 mm. Other recently published solutions can be found in [43], [44], [45], [46], [47], [48].

A possibility to enhance antenna diversity by redirecting radiation at desired locations is to use FSSs that introduce abrupt changes of phase when incident EM waves are reflected or refracted. This opportunity is based on the generalized laws of reflection and refraction [49], [29], which involves two media with different refractive indices (wavenumbers k_i and k_t respectively) and a linear phase gradient $\phi(x, y)$ that is supplementary introduced at the separation plane, Fig. 16.

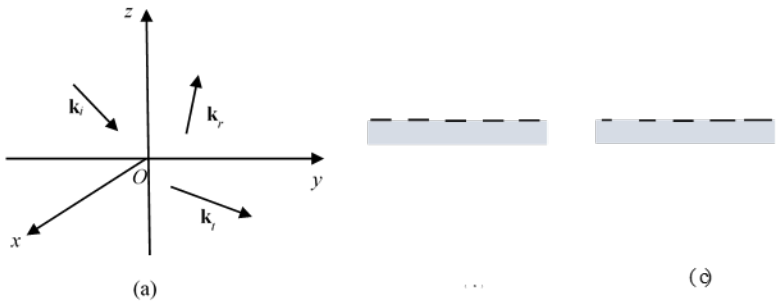

Fig. 16. Gradient FSSs: (a) anomalous reflection and refraction; (b) FSS with phase jump; (c) quasi-static approximation of gradient.

Suppose the separation plane is xOy in Fig. 16 (a) and the incident wavevector is in the zOy plane. Then

$$\begin{aligned} \boldsymbol{k}_i &= k_i(\boldsymbol{a}_y \sin\theta_i + \boldsymbol{a}_z \cos\theta_i) \\ \boldsymbol{k}_r &= k_r(\boldsymbol{a}_x \sin\theta_r \cos\phi_r + \boldsymbol{a}_y \sin\theta_r \sin\phi_r + \boldsymbol{a}_z \cos\theta_r) \\ \boldsymbol{k}_t &= k_t(\boldsymbol{a}_x \sin\theta_t \cos\phi_t + \boldsymbol{a}_y \sin\theta_t \sin\phi_t + \boldsymbol{a}_z \cos\theta_t) \end{aligned} \tag{5}$$

where the angles are referred to the spherical coordinate system associated to $Oxyz$, and $\boldsymbol{a}_x$ etc. are the unit vectors. Writing the phase matching in the xOy plane and tacking into account the phase gradient yields

$$\begin{aligned} 0 &= k_t \sin\theta_r \cos\phi_r - \phi'_x = k_t \sin\theta_t \cos\phi_t - \phi'_x \\ k_t \sin\theta_i &= k_i \sin\theta_r \psi_r - \phi'_y = k_t \sin\theta_t \psi_t - \phi'_y \end{aligned} \tag{6}$$

These equations can be solved for (θ_r, ϕ_r) and (θ_t, ϕ_t) to obtain the direction of anomalous reflection and refraction. Note that the laws of Snellius-Descartes result as a special case when the gradient is zero.

To implement gradient surfaces using FSSs some approximations must be made. The quasi-static approximation is most common. Consider a FSS that introduces a phase jump that depends on some geometrical parameter of the pattern, such as the length of an element or an angle of rotation, Fig. 16 (b), which covers the $(0, 2\pi)$ interval. Choose N discrete points in the $(0, 2\pi)$ interval and construct a new FSS having a unit supercell composed of N unit cells, each introducing the corresponding phase jump Fig. 16 (c). It is worth mentioning that the discretization of the gradient leads to the existence of regularly reflected and refracted beams [49]. The minimization of these waves and providing independency of the transmittance of the FSSs on the geometrical parameter involved to ensure a plane wave after anomalous reflection or refraction are major challenges for designers of gradient surfaces.

Various demonstrations of gradient surfaces have been reported in the literature. It is considered that the conception of reflectarrays and transmitarrays and of phased array antennas are essentially based on the same principle as the gradient surfaces [6].

4 Metasurfaces

A new perspective on FSSs has been introduced by the concept of Metasurfaces (MSs). Starting from the technical solutions relying on the concept of FSSs, researchers individualized the possibility of acting in a coherent manner on EM waves to control at will various parameters such as amplitude, phase, wavefront, polarization, and direction of propagation.

The theoretical foundations of MSs are based on some classical theorems in EMs: the uniqueness theorem, the Love-Schelkunoff equivalence principle, and the Huygens' principle.

The uniqueness theorem for a volume V bounded by a surface S states that the EM field at every point in the interior of V is determined by the tangent

component of the electric field intensity on S, or the tangent component of the magnetic field intensity on S, or by the tangent component of the electric field intensity on some part of S and the tangent component of the magnetic field intensity on the complementary part of S. The same boundary conditions determine the EM field in the volume V' situated at the exterior of S, provided that the field amplitudes decay at infinity faster than $1/r$, where r is the magnitude of the position vector referred to an arbitrarily selected origin.

The equivalence principle has been stated as follows in [7]: "a distribution of electric and magnetic currents on a given surface C can be found such that outside C it produces the same field as that produced by given sources inside C; and also, the field inside C is the same as that produced by given sources outside C. One of this system of sources can be identically equal to zero". The surface C is placed in a homogeneous medium.

Huygens' principle states that every point of a wavefront is a source of secondary waves and a new wavefront can be obtained as the envelope of the secondary outgoing waves. Combining the equivalence principle with Huygens' principle identifies the secondary sources as electric and magnetic surface current densities, which can be related to the tangent component of the electric and magnetic field at the given surface.

A MS is a FSS engineered such that imprinted or induced electric and magnetic current densities produce desired patterns of the emerging EM field from an incident EM wave [50]. In particular, if the MS is reflectionless, it is called a Huygens' MS. MSs that cancel both the transmitted and reflected fields are called absorbers. However, in most cases, the reflected and the transmitted fields are of interest. In this case, the surface current pattern must be engineered accordingly, Fig. 17 (a).

MSs find applications to spatial filtering, absorbers, polarization conversion (linear polarizers, linear-to-circular converters, polarization rotators), leaky-wave antennas, reflect- and transmitarrays, focusing, planar lens etc. Solutions with inclusion of active elements (switched or controlled MSs) have also been reported [51], [29], [52].

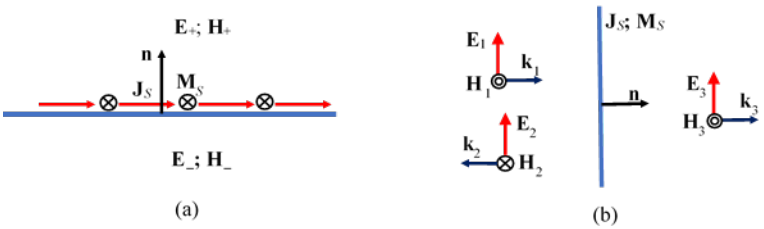

Fig. 17. Planar MS: (a) $\boldsymbol{J}_S$ – electric surface current density; $\boldsymbol{M}_S$ – magnetic surface current density; (b) plane waves in normal incidence.

The periodic character of the structure is lost in the EM characterization of MSs. Averaged values over the unit cell of the tangent electric and magnetic field intensities are used and effective surface parameters such as electric and magnetic susceptibilities are associated to the material. Obviously, such an approach holds if the wavelength is large as compared to the transversal dimensions and to the thickness of the unit cell [5]. Alternatively, an equivalent approach based on surface impedances and admittances can be considered [6].

An infinitely thin surface having a normal $\boldsymbol{n}$ and bearing surface electric current $\boldsymbol{J}_S$ and magnetic surface current $\boldsymbol{M}_S$ satisfy the boundary conditions (Fig. 17 (a)):

$$\begin{aligned} \boldsymbol{n} \times (\boldsymbol{H}_+ - \boldsymbol{H}_-) &= \quad \boldsymbol{J}_S \\ \boldsymbol{n} \times (\boldsymbol{E}_+ - \boldsymbol{E}_-) &= -\boldsymbol{M}_S \end{aligned} \tag{7}$$

where $\boldsymbol{E}_\pm$ and $\boldsymbol{H}_\pm$ are the field intensity vectors just above and below the surface in Fig. 17 (a) respectively. When the surface is thin, the tangential field intensity vectors $\boldsymbol{E}_t$ and $\boldsymbol{H}_t$ at the MS can be defined by [53], [6].

$$\begin{aligned} \boldsymbol{E}_t &= \tfrac{1}{2}(\boldsymbol{E}_{t+} + \boldsymbol{E}_{t-}) \\ \boldsymbol{H}_t &= \tfrac{1}{2}(\boldsymbol{H}_{t+} + \boldsymbol{H}_{t-}) \end{aligned} \tag{8}$$

where $\boldsymbol{E}_{t\pm}$ and $\boldsymbol{H}_{t\pm}$ are the tangent field intensity vectors above and below the surface.

The calculation of the tangent components of the fields must consider the variability on the surface of the unit cell. Average values over the surface of the unit cell S can be used, e.g.,

$$\boldsymbol{E}_{t\pm} = \frac{1}{S} \iint_S \boldsymbol{n} \times (\boldsymbol{E}_1 \times \boldsymbol{n}) \mathrm{d}S, \quad \text{etc.} \tag{9}$$

Modern CAD software allow for the estimations of the integrals. However, care must be taken to carry on the integration at a sufficient distance from the plane of the unit cell to avoid the influence of near field effects, but close enough to neglect the decay of the fields above or below the surface [54].

By linearity, the following two general tensor (or dyadic) relations can be written for the tangent components at the surface [6]:

$$\begin{aligned} \boldsymbol{E}_{t+} &= \underline{\boldsymbol{Z}}_{11} \cdot (\boldsymbol{n} \times \boldsymbol{H}_{t+}) + \underline{\boldsymbol{Z}}_{12} \cdot (\boldsymbol{n} \times \boldsymbol{H}_{t-}) \\ \boldsymbol{E}_{t-} &= \underline{\boldsymbol{Z}}_{21} \cdot (\boldsymbol{n} \times \boldsymbol{H}_{t+}) + \underline{\boldsymbol{Z}}_{22} \cdot (\boldsymbol{n} \times \boldsymbol{H}_{t-}) \end{aligned} \tag{10}$$

Equations (8) reduce e.g., in the case of the interface of a homogeneous medium with a metal of finite conductivity to the well-known approximate boundary condition that relate the tangent components of the field intensity vectors through the wave impedance of the metal. However, equations (8) bear a high degree of generality, since they account for magnetoelectric coupling [6]. Since four field vectors are involved in the interaction in Fig. 17 (a), other linear equations can be written that relate two of the quantities to the other two, involving various coefficients, by analogy to two-ports.

Consider the situation of Fig. 17 (b) with two plane waves incident to and one plane wave emerging from the MS, which carry surface currents that can be either impressed or induced by the incident fields. Denoting by η the wave impedance of the surrounding medium, the boundary conditions at the surface read:

$$\begin{aligned} \boldsymbol{n} \times (\boldsymbol{E}_3 - \boldsymbol{E}_1 - \boldsymbol{E}_2) &= -\boldsymbol{M}_S \\ \eta^{-1}\boldsymbol{n} \times (\boldsymbol{n} \times \boldsymbol{E}_3 - \boldsymbol{n} \times \boldsymbol{E}_1 + \boldsymbol{n} \times \boldsymbol{E}_2) &= \quad \boldsymbol{J}_S \end{aligned} \tag{11}$$

This equations system can be solved for the reflected wave $\boldsymbol{E}_2$ and the transmitted wave $\boldsymbol{E}_3$ by first cross multiplying at the left the first one by the normal unit vector $\boldsymbol{n}$. The solutions are as follows [6]:

$$\begin{aligned} \boldsymbol{E}_2 &= -\tfrac{1}{2}\eta\boldsymbol{J}_S - \tfrac{1}{2}\boldsymbol{n} \times \boldsymbol{M}_S \\ \boldsymbol{E}_3 &= \tfrac{1}{2}\boldsymbol{E}_1 + \tfrac{1}{2}\boldsymbol{n} \times \boldsymbol{M}_S - \tfrac{1}{2}\eta\boldsymbol{J}_S \end{aligned} \tag{12}$$

Note that the reflected wave vanishes if

$$\eta\boldsymbol{J}_S = \boldsymbol{M}_S \times \boldsymbol{n} \tag{13}$$

This condition states that the reflected wave is cancelled if the surface currents $\boldsymbol{M}_S$ and $\boldsymbol{J}_S$ are orthogonal and the ratio of their magnitudes is equal to the wave impedance of the surrounding medium. An MS that satisfies (13), which can be viewed as a matching condition, is called Huygens' surface. Huygens' surfaces are a solution of choice for controlling the wavefronts.

To characterize the interaction between the average EM field components (8) and the surface currents, separate linear tensor relations between $\boldsymbol{J}_S$ and $\boldsymbol{E}_t$ and between $\boldsymbol{M}_S$ and $\boldsymbol{H}_t$ are considered when no magnetoelectric interaction exist, with tensor impedance or admittance coefficients. When the surface currents are determined by both electric and magnetic field intensity vectors, the surface currents are linear combinations of the two, with tensor coefficients (the incident fields are preferred in this case rather than the average fields [6]). The impedance and admittance tensor coefficients are the effective parameters of the MS.

To generate magnetic surface currents, some conductive loops must be inserted in planes that are transversal to the MS. The thickness of the MS layer must be large enough to accommodate the loops. Electric currents that are induced (or imprinted) in the loops allow for the generation of the magnetic dipoles that are related to the magnetic current in a well-known way. In many situations, stacked layers of printed circuit boards are considered to allow for all functionalities required by the design specifications.

The above presented discussions concerning the operation and characterization of MSs have the goal to propose simplified models for a very complicated physical problem. A rigorous treatment of the interaction of EM waves with periodic surfaces must rely on the Bloch-Floquet theory. However, such an approach requires large computation resources and therefore cost-effective alternatives must be considered. It is important to be kept in mind the approximate character of the models and their limits of validity. Moreover, the impact of spatial dispersion might be important in some situations [53].

The retrieval of the effective surface parameters can be attempted in the context of the averaged approach. Another possibility is to retrieve the surface effective susceptibilities from the reflection and transmission coefficients of the MS in TE and TM incidence, in normal or oblique incidence [5].

MSs can be modulated by relying on the quasi-static approximation, Fig. 16 (b) and (c). An early solution has been introduced in the context of holographic antennas [54]. The necessary impedance pattern of a surface has been determined by calculating the interference pattern between surface currents generated by a small antenna and fields to ensure a given radiation. Then, after manufacturing the impedance sheet, the same currents launched over the surface by the small antenna radiate with the desired radiation pattern. The impedance pattern has been realized by means of square metal patches over one side of a dielectric sheet and covered with a ground plane on the other side (a PCB). For a constant dimension of the patches (the unmodulated case), surface impedance has been calculated by simulation. To avoid the effect of the decay of the field with the distance from the patches, the surface impedance has been defined as the average over the surface of the unit cell of the ratio of the tangent components of the electric and magnetic field intensities, in TM mode. In this way, fields at a quarter of a free space wavelength above the patches could be used to calculate the surface impedance, avoiding the errors that might be introduced by the near field, which is dependent on the "fine" structure of the surface. The obtained values for the impedance have been validated by comparison with results from other two methods, one relying on reflection and transmission coefficients and one on propagation theory of surface TM waves.

After the construction of a catalog of surface impedances in function of the dimensions of the patches, a modulated surface has been devised in the quasi-static approximation that implemented the holographic antenna. Both scalar and tensor impedance cases have been considered.

The literature reporting solution for enhancing antenna diversity and wave processing by means of MSs is huge and exponentially growing. The interested reader is referred to existing excellent reviews and the literature cited therein, e.g., [52], [51], [29], [5] [6] etc.

5 Interference in 5G communications

5G networks bring flexibility, optimization and include capabilities such as: multiple access technologies, network slicing, connectivity models, diversity mobility management and dynamic policy control. The networks operate mainly in mm-waves range (30-300 GHz) because spectrum between 700 MHz-2.6 GHz is congested, and above 6 GHz it is free. Also, in this frequency range more bandwidth is available and a higher throughput is possible.

In this paragraph, a discussion on EMC and different types of interferences that could appear in 5G networks is presented. The analysis starts with a literature review concerning interferences in the frequency bands of 5G networks. It is divided in four parts which cover the following topics: (i) FSSs with applications

in 5G bands, (ii) human exposure to electric field in different communication bands, (iii) EMC testing in 5G and (iv) interference between different communication systems.

5.1 Frequency Selective Surfaces with applications in 5G bands

As discussed above, FSS are EM structures that are periodic in a plane, in two directions and have a certain extent in the third, orthogonal direction. The FSSs spatial filtering properties are used to design effective screens that pass or cut signals from wireless local area network (WLAN), LTE, Bluetooth, industrial, scientific and medical (ISM), WiMax, or X-band. These filters can be: fixed, switchable (or active), and can be of wide- or narrow-band [55].

Furthermore, FSSs have found applications in filtering the bands that cover 5G spectrum in recent years [38], [56], [36], [37]. These reported FSSs are used to filter in the 28 GHz range [38], [56], [36], or 27.5 GHz [37].

The literature on the numerical analysis and description of experimental validations is quite large. Microwave Studio developed by CST [57] is used for example in [38], [56] and [37] as a tool to investigate these periodic structures, while other works, e.g., [36] report the use of HFSS by ANSYS [58] for EM simulations. In any cases, the analyses are based on Bloch-Floquet theory. From an application-oriented point of view, signal integrity (SI) issues, based on a cell phone model, are investigated for example in [56], because 5G communication systems and FSS might coexist.

Prototypes are fabricated, measured and their results are compared with the simulated ones in [38], [36] and [37]. Also, equivalent circuit models are validated in [36] and [37]. The response stability for TE and TM polarizations is investigated in [38] and [36] for incidences from 0 to 60°. Stable answer has been obtained for the considered configurations.

For example, for 5G EM shielding objective, an EM shielding design based on an FSS with vent holes has been recommended in [38]. The circular shape is the most common and efficient design for a vent hole to achieve the necessary ventilation and, based on this assumption, the authors proposed the following shapes: with one layer (split and slotted slit rings) and two layers (only with the design of slotted split rings) [38].

By optimizing the suggested FSS, it has achieved a bandwidth of more than 2 GHz, centered at 28 GHz, with 30 dB shielding efficiency (ratio of the electric field outside the shield without and with the presence of the shield) through a range of simulations using full-wave analysis provided by CST Microwave Studio. In order to achieve better shielding efficiency, a parametric analysis has been also conducted, including the variation of the incident angle (between 0 and 60°) for both TE and TM polarizations, which showed another advantage of this FSS: a good response stability. By comparing the measurement results of a prototype of the structure with the simulation data, a reasonable consistency has been obtained [38].

Authors of paper [56] proposed as EM shielding on 5G communication devices the use of FSSs. This solution aims to cause minimal effects on the 5G

communication, while enhancing the EMC performance of the device subjected to improvement (by reducing its emissions, and increasing the immunity). The unit cell that has been used was based on a circular pattern, and has been simulated in ANSYS HFSS. The effects of the FSS shielding in a 28 GHz 5×5 patch antenna array mounted on a generic smart phone have been investigated to resolve the issue of minimal interference with 5G communication. By undergoing a SI analysis on a DDR4 interface, the authors showed that it has not been affected by the presence of the FSS [56].

With the purpose of 5G EM Interference (EMI) shielding, a broadband bandpass FSS design has been proposed in [36]. The structure, intended to operate in the 28 GHz frequency band, had two transmission zeros and poles, and for miniaturization of the FSS, vias have been added. Thus, along the direction normal to the FSS, the surface current has been extended by the insertion of vias, and a 2.5-D periodic layer has been obtained with an air foam layer included. Cascading of several FSSs has also been tackled in this research to obtain a broad passband and also, for a deeper understanding, the concept of equivalent circuit model (ECM) has been applied. In the final part, to prove consistency for the recommended FSS, comparisons have been made between 3D simulations, a prototype having its functionality centered at 28 GHz and the ECM [36].

Finally, with the purpose of near-field 5G viable implementation, a low-profile broadband bandpass FSS with two rapid band edges has been proposed by the authors of [37]. Three metallic layers, separated by two thin substrates, formed the overall structure, which showed a good angular stability for both TE and TM modes. To better evaluate the concept of the proposed FSS, an ECM with a serial LC resonator has been introduced and an FSS prototype has been conceived. By experimenting with the prototype working at the frequency of interest (27.5 GHz), a 25 dB shielding efficiency has been obtained [37].

5.2 Human exposure to electric field in communications bands

Human exposure to electric field emitted in the communications frequency range has been of interest in the literature [59] - [61]. For example, bands such as LTE [59], Wi-Fi [60], [61] and GSM [61] have been tackled and spectrum measurements have been undergone.

Different scenarios have been considered: residential area near a base station [59], [60] and inside a train [61]. Electric field levels have been measured concerning: instantaneous exposure levels [59], also cumulative distribution functions have been calculated [60] and spatial distribution of the maximum electric field [61] has been evaluated.

The authors of [59] proposed a specification for evaluating the level of human RF exposure between 30 and 3000 MHz with an electric field (e-field) meter. Frequency spectrum measurements have been performed to assess these levels of exposure. Sleeve dipole elements were part of the proposed field meter, to help it achieve a sensitivity lower than 1 mV/m. Also, the e-field meter could measure the levels when mobile base stations (BSs) were using maximum transmission power for the transmitted signals [59].

As a case study, the total RF exposure level from 30 MHz to 3 GHz has been evaluated in a residential area situated near a mobile BS for LTE and W-CDMA systems. The maximum value of the total normalized maximum exposure levels has been less than the reference levels given in the ICNIRP guideline. The exposure level from the described mobile system and the target mobile BS were 13% and 10% of the total level at the maximum point, respectively. An uncertainty of 5.02 dB has been estimated using the proposed meter, in this case study. Finally, the exposure level in the assessment has been less than the reference e-field strength stipulated in the RF safety guideline even considering the uncertainty level [59].

Paper [60] provides guidelines on the safety enforcement evaluation considerations on the RF EM field, for 5G wireless networks. This work focuses on computational evaluation options in view of the fact that there are insufficient users to perform real life scenarios for 5G networks.The RF-EM field levels should be below the ICNIRP exposure limits so that wireless 5G networks can be effective [60]. An investigation that lead to plotts of cumulative distribution functions (CDF) of the field has been made in rural and urban areas with 64 antennas that comprised a MIMO array working at 3.5 GHz [60].

When using portable devices, during wireless data sharing with internet services, exposure to RF-EMF is unavoidable. The work [10] explored RF-EMF exposure profiles when using portable computers in fast-train vehicles. These trains studied in Poland did not have internal Wi-Fi facilities, and measurement have been done mostly in rural places [61]. By performing spectrum measurements in the GSM or Wi-Fi bands, the results showed that a worst-case scenario should be taken in consideration when evaluating wireless data exchange from portable computers. Also, this study verified that multi-path propagation of EMF signals may result in significantly higher RF-EM field exposure within train cars without internal Wi-Fi facilities than exposure from integrated wireless networks [61].

5.3 EM compatibility testing in 5G

The impact of EMC issues on 5G systems is of important interest. Various authors tackled this subject [62] - [66]. Topics such as far-field characterization of 5G antennas [62], interference impact on LTE from radiated emissions limits [63], measuring EM fields in 5G spectrum [64], LTE equipment performance evaluation [65] and methods to suppress noise emission in communication channels [66] have been considered.

Based on the above mentioned research, the following conclusions could be drawn: theoretical analysis showed that the far-field is formed much earlier in space [62], emission levels can cause severe impact on co-location [63], the new 5G methodology should consider factors such as massive MIMO, precise beam forming and new antenna radiation patterns should be considered [64]. A method to apply an invert calibration matrix to the input signal of the throughput test has been proposed [65] and improvement of LTE communication performance by means of magnetic composite sheets has been considered [66].

Antenna arrays and beam-steering techniques in the millimeter-wave region are powered by 5G mobile devices and base stations [62]. For these systems, the issue of far-field measurement distance is especially important, as a wider over-the-air test range implies dynamic range problems and considerably higher costs. The physical significance of a measurement distance greater than 6 meters has been examined in [62], with a case study consisting of measurements done for a smartphone operating at 39 GHz.

The authors of [62] presented the hypothesis that the far-field behavior is developed much earlier in space and they used measurement data to support these results. An anechoic chamber has been used for measurements which had the purpose to derive new expressions for much shorter far-field distances [62].

In a wide range of sectors, society is increasingly dependent on LTE services, which is why there is a need to be assured that these services are secure, being sensitive to radiated EMI, just like any wireless technology. The authors of [63] illustrated that, if we discuss about co-location distances above one meter (MIL-STD-461 standard) or of above 20 meters (EN55022), the levels of radiated emissions limits from the aforementioned standards, will cause a significant effect on LTE [63].

EM fields issues will become one of the main aspects of the cost-effective set-up of the 5G infrastructure [64], because by installing a large number of densely located base stations operating in the millimeter-wave range, the latest 5G networks would satisfy the stringent demand for bandwidth, but could cause problems regarding the exceeding of exposure limits to EM field. This is supported by the fact that there already exist sources of perturbation, such as previously created mobile technologies [64].

Analyses that are important for the evaluation of EM field compliance with regulatory limits have been included in [64], discussing topics that are relevant to measurements in 5G networks. For EM field measurements in the 5G network, one should take into account different factors such as: precise beam forming, time-division duplexing (TDD) access to the medium or massive MIMO, factors that are not used in 2G, 3G or 4G technologies. A negative effect on the roll out of the 5G network could appear because of the above-mentioned aspects, together with the stringent EM field limits regulations which are in use in a few countries. To solve the problem of reaching the network performances, calculations and simulations have been performed to get a better insight on the EM field distribution [64].

One of the approaches suggested to standard organizations is the two-stage approach for LTE MIMO wireless user equipment (UE) efficiency evaluation [65]. Two problems have been addressed by the authors of [65] regarding the conducted two-stage method: in the throughput test, there exists an interference between the device under test (DUT) and the method itself, and secondly, this method does not offer support for "over-the-air" (OTA). So, a solution is proposed by means of the so-called radiated two-stage (RTS) method, which can lead to enhancing the accuracy of a test.

This RTS method eliminates the key weaknesses of two-stage conducted method and preserves all its benefits [65]. For example, the problem of connecting the RF cable directly to the DUT receiver is removed, because the proposed method conducts an OTA second stage test by applying the invert calibration matrix to the input signal of the throughput test. Another advantage could be that in a typical single-input-single-output (SISO) anechoic chamber, this RTS OTA MIMO test method can be performed. This will offer comprehensive information at the sub-component level, decrease device expenses and offer good predictability, being an excellent solution for certification testing [65].

To improve the efficiency of LTE communication, magnetic composite sheets have been proposed in [66]. Also, this technique has been tested for the strength of noise emissions from a chip and it lead to noise suppression [66]. If the magnetic composite ferrite sheets cover the front-side of a chip, this material absorbs the EM wave that comes from the operating circuit. Thus, the unwanted RF noise emissions are removed. The effectiveness of the material was found to be composite dependent. For example, to achieve an improvement in efficiency in the 800 MHz frequency range of approximately 8 dB, BaZn-Y hexagonal ferrites are recommended to be used. Measurements and simulations have been performed to demonstrate this impact [66].

5.4 Interference between different communications systems

Interference between communications systems related to 5G spectrum has gained interest in the literature. Immunity of these systems have therefore been studied [67]-[74]. For signal generating the following solutions have been considered: software defined radio (SDR) [67], LTE signal generator [68], [69], arbitrary waveform generator [71]. Some of the authors have performed measurements in a specific anechoic chamber [67], or a reverberation chamber [68], [69].

Also, measurements have been performed in different frequency bands: 5 GHz band [67], between 600-800 MHz [68], [69], [73], around 2500-2600 MHz [71], [73] and between 2500-5000 MHz [74]. Furthermore, devices have been exposed to broadband perturbation signal [68], [69] or CW signals [72]. Finally, the studies have been concerned with orthogonal frequency division multiplexing (OFDM) [70], [72], [74], Error Vector Magnitude [71], Interference to Noise criteria and Bit Error Rate (BER) [74].

Because market leaders are quickly adopting the exploitation of unlicensed spectrum bands for cellular communication, the LTE-Licensed Assisted Access (LAA) appeared as an extension to LTE requirements, to enable unlicensed spectrum operation. A case study concerning wireless coexistence testing is reported in [67] concerning experiments carried out at the U.S. Food and Drug Administration's EM Compatibility and Wireless Laboratory. It is common knowledge that LTE systems can interfere with unlicensed spectrum consumers (for example wireless medical devices), so to generate practical LAA signals and calculate the wireless coexistence effect on LAA communication, a SDR platform was deployed [67].

Measurement tests were performed inside an anechoic chamber in the 5 GHz frequency band. Results suggest that if maximum possible modulation and coding system as well as maximum possible channel time occupancy are implemented, the LAA signal will have the strongest impact on coexistence capabilities for the equipment under test (EUT). Even if the EUT is in the medical area, it could be helpful to make use of unlicensed wireless spectrum technology (Bluetooth, Wi-Fi) [67].

To test the immunity of electronic components to radiated signals, a reverberation chamber has been suggested, because different polarization and incident angles can be achieved when exposing the DUT. During normal service, these types of devices can be exposed to broad- or narrow-band signals [68].

While the exposure to narrow-band signals is well documented, there is an increasing interest in the proper operation of the DUT when exposed to a broadband signal, because of the rise of broad-band communication technologies. With the purpose of analyzing the potential for 4G/LTE signal interference, measurements of cable television devices have been used in the case study from [68]. Investigations have been made regarding reasons why the output of the device is dramatically changed when exposed to broadband signals [68].

When tackling immunity of an electronic device, if we take into consideration a narrow-band signal compared to a broad-band one, different approaches must be considered in testing [69]. The authors from [69] identified some challenges in previous publications: deciding when a DUT has a fail, selecting a specific measuring area by relying on experiments. The authors continued these experiments involving cable communications equipment and the sensitivity to radiated LTE signals in [69], and changed the emphasis to proposed answers to these issues.

The interference and EMC topics related to the coexistence of LTE with other networks have been illustrated in [70], given the fact that in the 3GPP LTE networks, OFDM technique is used. The loss of efficiency due to coexistence has been presented by means of different RF scenarios and solutions to improve this coexistence have been proposed in terms of frequency assignment and transmission scheme [70].

An overview of the vulnerability of the LTE physical layer in the presence of jamming signals has been provided by the authors of [71]. Commercial jammers are identified by the swept frequency bands and by the sweep length that can be distinct according to the jammer model, the jamming signal typically using a fixed sweep time. In the paper, in order to examine the troubling mechanisms, the authors have reviewed the possible impact of jamming signals according to their emission power. By measuring three parameters: Occupied Bandwidth (OBW), Error Vector Magnitude (EVM), and Adjacent Channel Leakage-power Ratio (ACLR), the quality of the LTE uplink has been analyzed [71].

Like mentioned before, recently OFDM was included in the 5G mobile device standard, being used previously in a variety of networks related to broadcasting: digital video broadcasting (DVB) and digital audio broadcasting (DAB) or in networks like WLANs of LTE mobile systems [72].

The immunity of 5G networks to various forms of CW interference (a single CW signal or multiple synchronized CW signals) is tackled in [72]. In order to approximate parameters from the 5G standard, OFDM and error correction codes have been included in the analyzed framework. The findings in this research tackled also the subject of limiters in time domain (decreasing the impact of many CW signals interfering) and frequency domain (minimization of the impact of a single CW signal). Comparisons made with white Gaussian noise showed that it had a stronger impact on the 5G network than the CW interferer [72].

In 2011, all interested parties were invited by the Swedish regulator (PTS) to apply for licenses (which should provide Mobile Broadband – MBB over LTE Standard) for the use of radio transmitters in the 790-862 MHz frequency band [73]. PTS has placed a range of technical restrictions on the licenses in order to protect the Digital Terrestrial Television (DTT) services offered in the adjacent bands from interference.

A brief description of these technical conditions is given in [73], and a measurement campaign has been carried out to examine the interference between MBB and DTT services. The measurement results lead to the following conclusions: the technical specifications provide the MBB downlink as envisioned by PTS with additional security for DTT reception and MBB services can suffer from TV Channel 60 interference within a radius of about 5 km from the DTT transmitter [73]. The regulator received relatively few complaints one year after the rollout of MBB services in the Swedish 800 MHz band, due to the fact that the licensees have provided additional filters free of charge in situations where interference with the TV reception has occurred [73].

Finally, having a variety of applications for ultrawideband (UWB) systems, and given the rapid development of OFDM-based wireless communication systems, analysis on the coexistence of these two kinds of systems has been considered of great interest. Consequently, the authors of [74] using physical layer modeling strategy in Simulink devised the UWB model on one side, and IEEE802.11n, WiMAX, and LTE downlink systems models on the other side. The simulation results were compared by considering the interference to noise ratio (I/N) procedure [74].

References

1. Wang T., Li G., Ding J., Miao Q., Li J., Wang Y.: 5G Spectrum: Is China Ready?. IEEE Comm. Mag., **53**(7), 58–65, (2015)
2. Petosa, A.: Engineering the 5G environment, IEEE 5G World Forum, 478–481, IEEE, Silicon Valley, CA, USA, 2018
3. Rappaport T.S. et al.: Millimeter wave mobile communications for 5G Cellular: It will work!, IEEE Access, 1, 335–349, (2013)
4. Chen M., Kim M., Wong A.M.H., Eleftheriades G.V.: Huygens' Metasurfaces form Microwaves to Optics: a review. Nanophotonics, **7**(6), 1207–1231, (2018)
5. Holloway, C.L., Kuester, E.F., Gordon, J.A., O'Hara, J., Booth, J., Smith, D.R.: An overview of the theory and applications of metasurfaces: the two-dimensional equivalents of metamaterials. IEEE Antennas Propag. Mag., **54**(2), 10–34, (2012)
6. Tretyakov, S.A.: Metasurfaces for general transformations of EM fields. Phil. Trans. R. Soc. A, 373: 20140362, (2015)
7. Schelkunoff, S: Some equivalence theorems of EMs and their application to radiation problems. Bell Syst. Tech. J., 15, 92–112, (1936).
8. Shelby, R.A., Smith, D.R., Schults, S.: Experimental verification of a negative index of refraction. Science 292, 77–79 (2001)
9. Pendry, J.B., Holden, A.J., Robbins, D.J., Stewart. W.J.: Magnetism from conductors and enhanced nonlinear phenomena. IEEE Trans. Microw. Theory Techn., **47**(11), 2075–2084, (1999)
10. Eleftheriades, G.V., Balmain, K.G.: Negative-Refraction Metamaterials. IEEE/Wiley, Hoboken NJ, USA (2005)
11. Alù A., Engheta N.: Achieving transparency with plasmonic and metamaterial coatings. Phys. Rev. E 72, 016623 (2005)
12. Caloz C., Itoh T.: EM Metamaterials: Transmission Line Theory and Microwave Applications. IEEE/Wiley, Hoboken NJ, USA (2006)
13. Brillouin, L.: Wave Propagation in Periodic Structures, Dover, New York (1953)
14. Sievenpiper, D., Zhang, L., Boas, F. J., Alexópoulos, N. G., Yablonovitch, E.: High-impedance EM surfaces with a forbidden frequency band. IEEE Trans. Microw Theory Tech., **47**(11), 2059–2074, (1999)
15. Clavijo, S., Diaz, R.E., McKinzie III, W.E.: Design methodology for Sievenpiper high-impedance surface: an artificial magnetic conductor for positive gain electrically small antennas. IEEE Trans. Antennas Propag., **51**(10), 2678–2690, (2003)
16. Jackson, D.R., Oliner, A.A.: Leaky Wave Antennas. In Balanis C.A. (ed.): Modern Antenna Handbook, Wiley, NJ (2008)
17. Abhari, R., Eleftheriades, G.V.: Metallo-dielectric EM band-gap structures for suppression and isolation of the parallel-plate noise in high-speed circuits. IEEE Trans Antennas Propag., **51**(6), 1629–1639, (2003)
18. Rogers, S. D.: EM-bandgap layers for broad-band suppression of TEM modes in power planes. IEEE Trans. Microw. Theory Tech., **53**(8), 2495–2505, (2005)
19. De Sabata, A., Matekovits, L.: EM Band-Gap Solution for Mitigation of Parallel-Plate Noise in Power Distribution Networks. Microw. Optical Tech. Lett., **54**(7), 1689–1692, (2012)
20. Williams, D.F.: Damping of resonant modes of a rectangular metal package. IEEE Trans. Microw. Theory Tech., **37**(1), 253–256, (1989)
21. Rajo-Iglesias, E., Zaman, A.U., Kildal, P.-S.: Parallel-plate cavity mode suppression in microstrip circuit packages using lid of nails. IEEE Microw. Wireless Compon. Lett., **20**(1), 31–33, (2010)

22. Matekovits, L., De Sabata, A.: Signal Integrity Applications of an EBG Surface. Advances in Electrical and Computer Engineering, **15**(2), 3–8, (2015)
23. De Sabata, A., Matekovits, L.: Unit cell geometry in stripline technology featuring sequential band-gaps between every two consecutive modes. IEEE Antennas Wireless Propag. Lett., 11, 97–100 (2012)
24. Matekovits, L., De Sabata, A., Esselle, K.P.: Effects of a coplanar waveguide biasing network built into the ground plane on the dispersion characteristics of a tunable unit cell with an elliptical patch and multiple vias. IEEE Antennas Wireless Propag. Lett., 10, 1088–1091, (2011)
25. De Sabata, A., Matekovits, L.: Reduced complexity biasing solution for switched parallel-plate waveguide with embedded active metamaterial layer. Journal of Electromagn. Waves and Appl. (JEMWA), **26**(14/15), 828–1836, (2012)
26. Matekovits, L., De Sabata, A., Orefice, M.: Parametric study of a unit cell with elliptical patch for periodic structures with variable number of grounding vias. Proc. of the Fourth Eur. Conf. Antennas Propag. (EUCAP), 1-3 Barcelona, Spain, 1–3, (2010)
27. Munk, B.A.: Frequency-Selective Surfaces – Theory and Design. Wiley, New York (2000)
28. Mackay, J. A., Sanz-Izquierdo, B., Parker, E.A.: Evolution of Frequency Selective Surfaces. Forum for Electromagn. Res. Methods Appl. Technol. (FERMAT), 2, 1–7, (2014)
29. Chen, H.-T., Taylor, A.J., Yu, N.: A review of metasurfaces: physics and applications. Rep. Prog. Phys., 79, 076401 (40 pp.), (2016)
30. Anwar, R.S., Mao, L., Ning, H.: Frequency selective surfaces: a review. Appl. Sci., 8, 1689, 47 pp., (2018)
31. Costa, F., Monorchio, A., Manara, G.: An overview of equivalent circuit modeling techniques of frequency selective surfaces and metasurfaces. ACES Journal, **29**(12), 960–976, (2014)
32. Syed, I.S., Ranga, Y., Matekovits, L., Esselle, K.P., Hay, S.G.: A single layer frequency-selective surface for ultrawideband EM shielding. IEEE Trans. Electromag. Compat., **56**(6), 1404–1410, (2014)
33. Valerio, G., Ghasemifard, F., Sipus, Z., Quevedo-Teruel, O.: Glide-symmetric all-metal holey metasurfaces for low-dispersive artificial materials: Modeling and properties. IEEE Trans. Microw. Theor. Techn., **66**(7), 3210-3223, (2018)
34. Matekovits, L., De Sabata, A., Silaghi, A.: Frequency selective surface with two quasi-independent notch frequencies. IEEE Access, **7**(1), 77261–77267, (2019)
35. Luukonen, O., Simovski, C., Granet, G., Goussetis, G., Lioubttchenko, D., Räisänen, A., Tretyakov. S.A.: Accurate analytical model of planar grids and high-impedance surfaces comprising metal strips or patches. IEEE Trans. Antennas Propag., **56**(6), 1624–1632, (2008)
36. Li, D., Li, T.-W., Li, E.-P., Zhang, Y.-J.: A 2.5-D angularly stable frequency selective surface using via-based structure for 5G EMI shielding. IEEE Trans. Electromagn. Compat., **60**(3), 768–775, (2018)
37. Li, D., Li, T.-W., Hao, R., Chen, H.-S., Yin, W.-Y., Yu, H.-C., Li,, E.-P.: A low-profile broadband bandpass frequency selective surface with two rapid band edges for 5G near-field applications. IEEE Trans. Electromagn. Compat., **59**(2), 670–676, (2017)
38. Yan, L., Xu. L., Zhao, X., Gao, R.X.-K.: An angularly stable frequency selective surface with vent holes for 5G EM shielding. In: Proc. of the 2019 International Symposium on EM Compatibility (EMC Europe 2019), pp. 366–369. IEEE, Barcelona, Spain, (2019)

39. Sivasamy, R., Moorthy, B., Kanagasabai, M., Samsingh, V.R., Alsath, M.G.N.: A wideband frequency tunable FSS for EM shielding applications. IEEE Trans. Electromag. Compat., **60**(1), 280–283, (2018)
40. Silaghi, A., De Sabata, A., Matekovits L.: Frequency selective surfaces for dual band polarizer in automotive. APS/URSI 2019, 1–4, Georgia, USA, (2019)
41. Fei, P., Shen, Z., Wen, X., Nian, F.: A single-layer circular polarizer based on hybrid meander line and loop configuration. IEEE Trans. Antennas Propag., **63**(10), 4609–4613, (2015)
42. Fahad, A.K.F., Ruan, C., Nazir, R., Saleem, M., Haq, T.U., Ullah, S., He, W.: Ultra-thin metasheet for dual-wide-band linear to circular polarization conversion with wide-angle performance. IEEE Access, Early Access, (2020)
43. Arnieri, E., Greco, F., Amendola, G.:A broadband, wide angle scanning, linear to circular polarization converter based on standard Jerusalem-cross frequency selective surfaces. IEEE Trans. Antennas Propag., Early Access, (2020)
44. Baena, J.D., Glybowski, S.B., del Risco, J.P., Slobozhanyuc, A.P., Belov, P.A., Broadband and thin linear-to-circular polarizers based on self-complementary zigzag metasurfaces. IEEE Trans. Antennas Propag., **65**(8), 4124–4133, (2017)
45. Li, H., Li, B., Zhu, L.: Wideband linear-to-circular polarizer based on orthogonally inserted slot-line structures, IEEE Antennas Wireless Propag. Lett, **18**(6), 1169–1173, (2019)
46. Zeng, Q., Ren, W., Zhao, H., Xue, Z., Li, W.: Dual-band transmission-type circular polariser based on frequency selective surfaces. IET Microw. Antennas Propag., **13**(2), 216–222, (2019)
47. Zhang, H.-F., Zeng, L., Liu, G.-B., Huang, T.: Tunable linear-to-circular polarization converter using the graphene transmissive metasurface, IEEE Access, 7, 158634–158642, (2019)
48. Wang, H.B., Cheng, Y.J.: Single-layer dual-band linear-to-circular polarization converter with wide axial ratio bandwidth and different polarization modes, IEEE Trans. Antennas Propag., **67**(6), 4296–4301, (2019)
49. Yu, N., Genevet, P., Kats, M.A., Aieta, F., Tetienne, J.-P., Capasso, F., Gaburro, Z.: Light propagation with phase discontinuities: generalized laws of reflection and refraction. Science, 334, 333–337, (2011)
50. Pfeiffer, C., Grbic, A.: Metamaterial Huygens' surfaces: tailoring wave fronts with reflectionless sheets. Phys. Rev. Lett., 110, 197401, (2013)
51. Glybovski, S.B., Tretyakov, S.A., Belov, P.A., Kivshar, Y.S., Simovski, C.R.: Metasurfaces: from microwaves to visible. Phys. Rep. 634, 1–72, (2016)
52. V. G. Ataloglou, M. Chen, M. Kim and G. V. Eleftheriades.: Microwave Huygens' metasurfaces: fundamentals and applications. IEEE J. Microw, **1**(1), 374–388, (2020)
53. Tretyakov, S.: Analytical modeling in applied EMs. Artech House Norwood, MA (2003)
54. Fong, B.H., Colburn, J.S., Ottusch, J.J., Visher, J.L., Sievenpiper, D.F.: Scalar and tensor artificial impedance surfaces. IEEE Trans. Antennas Propag., **58**(10), 3212–3221 (2010)
55. Buta, A., De Sabata, A., Iftode, C., Silaghi, A., Matekovits, L.: Applications of a Frequency Selective Surface Based on a Combination of Jerusalem Cross and a Circular Ring. 2018 International Conference on Communications (COMM), pp. 239–242, 14-16 June 2018. IEEE, Bucharest, Romania (2018)
56. Mologni, J., Ribas, J., Junior, A., Alves, M.: Investigation on the Deployment of FSS as EM Shielding for 5G devices. 2017 SMBO/IEEE MTT-S International

Microwave and Optoelectronics Conference, pp. 1–4, 27-30 Aug. 2017. IEEE, Aguas de Lindoia, Brazil (2017)
57. CST Microwave Studio, www.3ds.com
58. ANSYS HFSS, ansys.com
59. Higashiyama, J., Tarusawa, Y.: Design of Electric Field Meter to Assess Human Exposure in Environment with Mobile Base Station. 2014 International Symposium on EM Compatibility, pp. 650–653, 12-16 May 2004. Tokyo, Japan (2004)
60. Rumeng, T., Ying, S., Tong, W., Wentao, Z.: EM field safety compliance assessments for 5G wireless networks. 2020 International Symposium on EM Compatibility & Signal/Power Integrity (EMCSI 2020), pp. 659–662, 28 July -28 Aug. 2020. IEEE, Reno, USA (2020)
61. Gryz, K., Karpowicz, J.: Radiofrequency EM exposures during the use of wireless links of portable computers inside trains without internal WiFi services. 2019 International Symposium on EM Compatibility (EMC Europe 2019), pp. 1030–1033, 2-6 Sept. 2019. IEEE, Barcelona, Spain (2019)
62. Derat, B.: 5G Antenna Characterization in the Far-Field. 2018 International Symposium on EM Compatibility and 2018 IEEE Asia-Pacific Symposium on EM Compatibility (EMC/APEMC 2018), pp. 959–962, 14-18 May 2018. IEEE, Singapore, Singapore (2018)
63. Stenumgaard, P., Fors, K., Wiklundh, K.: Interference Impact on LTE from Radiated Emissions Limits. 2015 IEEE International Symposium on EM Compatibility (EMC 2015), pp. 165–170, 16-22 Aug. 2015. IEEE, Dresden, Germany (2015)
64. Pawlak, R., Krawiec, P., Zurek, J.: On measuring EM Fields in 5G Technology. IEEE Access, **7**, pp. 29826–29835, IEEE (2019)
65. Yu, W., Qi, Y., Liu, K., Xu, Y., Fan J.: Radiated Two-Stage Method for LTE MIMO User Equipment Performance Evaluation. IEEE Trans. Electromagn. Comp., **56**(6), pp. 1691–1696, (2014)
66. Watanabe, K., Jike, K. et al.: Magnetic Composite Sheets in IC Chip Packaging for Suppression of Undesired Noise Emission to Wireless Communication Channels. 2019 12th International Workshop on EM Compatibility of Integrated Circuits (EMC Compo 2019), pp. 219–221, 21-23 Oct. 2019, Hangzou, China (2019)
67. Kalaa, M., Seidman, S.: Wireless Coexistence Testing in the 5GHz Band with LTE-LAA Signals. 2019 IEEE International Symposium on EM Compatibility, Signal & Power Integrity (EMC+SIPI 2019), pp. 437–442, 22-26 July 2019. IEEE, New Orleans, USA (2019)
68. Coder, J., Ladbury, J., Hunter D.: Characterizing a Device's Susceptibility to Broadband Signals: A Case Study. 2014 IEEE International Symposium on EM Compatibility (EMC 2014), pp. 295–300, 4-8 Aug. 2014. IEEE, Raleigh, USA (2014)
69. Coder, J., Ladbury, J., Young, W.: Measuring a Device's Susceptibility to LTE: Preliminary Approaches. 2015 IEEE Symposium on EM Compatibility and Signal Integrity (EMC 2015), pp. 63–68, 15-21 March 2015. IEEE, Santa Clara, USA (2015)
70. Dong, Z., Di, J., Shuping, C., Mugen, P., Wenbo, W.: Interference Analysis and Co-existence Studies of 3GPP LTE Systems. 2007 International Symposium on Microwave, Antenna, Propagation and EMC Technologies for Wireless Communications, pp. 200–204, 16-17 Aug. 2007. Hangzou, China (2007)
71. Romero, G., Deniau, V., Stienne, O.: LTE Physical Layer Vulnerability Test to Different Types of Jamming Signals. 2019 International Symposium on EM Compatibility (EMC Europe 2019), pp. 1138–1143, 2-6 Sept. 2019. IEEE, Barcelona, Spain (2019)

72. Fors, K., Axell, E., Linder, S., Stenumgaard, P.: On the Impact of CW interference on 5G NR. 2019 International Symposium on EM Compatibility (EMC Europe 2019), pp. 1049–1054, 2-6 Sept. 2019. IEEE, Barcelona, Spain (2019)
73. Elofsson, C., Karlsson, C., Beckman, C.: On The Interference between Digital Terrestrial Television and Mobile Broadband in the Swedish 800 MHz Band. 2014 International Symposium on EM Compatibility (EMC Europe 2014), pp. 528–532, 1-4 Sept. 2014. IEEE, Gothenburg, Sweden (2014)
74. Zou, Z., Zou, W., Li, B., Zhou, Z., Huang, X.: Analysis on Coexistence of Ultra Wideband with OFDM-Based Communication Systems. IEEE Trans. Electromagn. Comp., **53** (3)pp. 823–830 (2011)